Am J Cancer Res 2024;14(3):996-1014
www.ajcr.us /ISSN:2156-6976/ajcr0152190

Original Article

Comprehensive analysis identifies long non-coding RNA RNASEH1-AS1 as a potential prognostic biomarker and oncogenic target in hepatocellular carcinoma

Jin Sun[2,3,4], Yingnan Li[4], Hongwei Tian[2,3,4], Haiyan Chen[2,5], Jun Li[2,3,4], Zongfang Li[1,2,3,4]

[1]Department of General Surgery, The Second Affiliated Hospital of Xi'an Jiaotong University, Xi'an, Shaanxi, China; [2]National and Local Joint Engineering Research Center of Biodiagnostics and Biotherapy, Xi'an Jiaotong University, Xi'an, Shaanxi, China; [3]Shaanxi Provincial Clinical Research Center for Hepatic and Splenic Diseases, The Second Affiliated Hospital of Xi'an Jiaotong University, Xi'an, Shaanxi, China; [4]Center for Tumor and Immunology, The Precision Medical Institute, Xi'an Jiaotong University, Xi'an, Shaanxi, China; [5]Core Research Laboratory, The Second Affiliated Hospital of Xi'an Jiaotong University, Xi'an, Shaanxi, China

Received July 13, 2023; Accepted February 22, 2024; Epub March 15, 2024; Published March 30, 2024

Abstract: RNASEH1-AS1, a long non-coding RNA (lncRNA) divergently transcribed from the antisense strand of its neighboring protein-coding gene ribonuclease H1 (RNASEH1), has recently been demonstrated to be involved in tumor progression. However, the association between RNASEH1-AS1 and hepatocellular carcinoma (HCC) remains unclear. In the present study, first, the expression of RNASEH1-AS1 in HCC and its correlation with clinicopathological features, prognosis, diagnosis, immune cell infiltration of HCC patients was inspected using relevant R packages based on The Cancer Genome Atlas (TCGA) data. RNASEH1-AS1 was found to be up-regulated in most cancer types, including HCC, and its overexpression was significantly associated with histologic grade and AFP level as well as poor prognosis, and was an independent risk factor affecting overall survival with good diagnostic and prognostic values for HCC. RNASEH1-AS1 was inversely associated with the infiltration of most immune cell types, including plasmacytoid dendritic cells (pDC), B cells and neutrophils. Second, a total of 1109 positively co-expressed genes (PCEGs) of RNASEH1-AS1 were screened out in HCC by correlation analysis in batches (|Spearman's r| >0.4 and adjusted *P* value <0.01). GO and KEGG enrichment analysis indicated that PCEGs of RNASEH1-AS1 were mainly related to RNA processing, ribosome biogenesis, transcription and histone acetylation. The top 10 hub genes (EIF4A3, WDR43, WDR12, DKC1, NAT10, UTP18, DDX18, BYSL, DDX10, PDCD11) were identified by constructing the protein-protein interaction (PPI) network, and they were all highly expressed in HCC and positively correlated with histological grade. Third, a risk model was constructed based on four RNASEH1-AS1-related hub genes (EIF4A3, WDR12, DKC1, and NAT10) with good prognostic predictive potential via univariate Cox and the least absolute selection operator (LASSO) regression analysis. Fourth, experimental validation revealed that RNASEH1-AS1 was significantly elevated in HCC tissues and several cell lines, and its knockdown could suppress the proliferation, migration, and invasion of HCC cells. Finally, mechanistic studies demonstrated that the stability of RNASEH1-AS1 could be regulated by DKC1 via their direct interaction. Taken together, RNASEH1-AS1 may serve as a potential prognostic and diagnostic biomarker and oncogenic lncRNA for HCC.

Keywords: Hepatocellular carcinoma, RNASEH1-AS1, prognosis, diagnosis

Introduction

Hepatocellular carcinoma (HCC), the principal histologic type of primary liver cancer, ranks the sixth in the global cancer incidence and the third leading cause of cancer-related death, and its incidence continues to increase worldwide [1, 2]. Early-stage HCC patients can be effectively treated by surgical resection, liver transplantation or radiofrequency ablation. However, most HCC patients have already entered the middle and late stages when they are first diagnosed and have lost the opportunity for radical treatment [3, 4]. In recent years, molecular targeted drugs (such as sorafenib, lenvatinib, etc.) and immune checkpoint inhibitors (such as PD-L1 and PD-1 inhibitors, etc.) have achieved certain effects in HCC treat-

https://doi.org/10.62347/JPHF4071

ment, but the overall effect is not ideal [5-7]. Thus, more effective biomarkers and therapeutic targets for HCC need to be urgently developed.

Long non-coding RNA (lncRNA) is a kind of RNA molecule with length more than 200 nucleotides and lacks protein coding ability. Most lncRNAs are transcribed by RNA polymerase II (Pol II) and structurally similar to mRNAs (capped, spliced and polyA tail) [8]. LncRNA can modulate gene expression at epigenetic, transcriptional, and post transcriptional levels through interacting with DNA, mRNA, protein, and microRNA (miRNA) to be involved in a wide variety of diseases, including solid and hematological tumors [9-11]. For HCC, a large number of lncRNAs have been identified to be aberrantly expressed in HCC and contribute to tumor development by affecting various biological processes such as cell proliferation, apoptosis, migration, invasion, angiogenesis and drug resistance, exhibiting their potential as prognostic and diagnostic biomarkers as well as therapeutic targets for HCC [12-14].

RNASEH1-AS1, also known as RNASEH1-DT, is an lncRNA divergently transcribed from the antisense strand of its neighboring protein-coding gene ribonuclease H1 (RNASEH1) which located on human chromosome 2 at 2p25.3. RNASEH1-AS1 has been found to be abnormally expressed in several cancers, such as lung squamous cell carcinoma [15], ovarian cancer [16], non-small cell lung cancer (NSCLC) [17]. A recent study demonstrated that RNASEH1-AS1 contributed to the NSCLC progression as an oncogenic molecule, suggesting that RNASEH1-AS1 may play important roles in the occurrence and development of tumors [17]. However, it is still not clear whether RNASEH1-AS1 is abnormally expressed in HCC and whether it is involved in the HCC progression.

In this study, the expression status of RNASEH1-AS1 and its potential clinical significance, biological functions, and molecular mechanisms in HCC were comprehensively investigated for the first time through bioinformatics analysis and wet-lab experiments validation. In brief, the current study aims to provide a basis for the application of RNASEH1-AS1 in the diagnosis and prognosis of HCC, as well as its functional and mechanistic studies.

Materials and methods

Data acquisition and processing

Toil recomputed RNA-sequencing (RNA-seq) data (TCGA and GTEx) of 30 types of cancers were downloaded from UCSC XENA (https://xenabrowser.net/datapages/) for pan-cancer analysis and the number of samples for each cancer is shown in Supplementary Table 1. The RNA-seq data and clinical information of 370 HCC patients were gathered from the TCGA data repository (https://portal.gdc.cancer.gov/repository) for further analysis and a summary of the clinical information of HCC patients is provided in Supplementary Table 2. Besides, the expression matrix of GSE45436, GSE84402, GSE55092, GSE29721 datasets was downloaded from the GEO database (https://www.ncbi.nlm.nih.gov/geo/) to validate the expression of RNASEH1-AS1 in HCC tissues and normal tissues.

Bioinformatics analysis of RNASEH1-AS1 expression and its clinical significance in HCC

The expression of RNASEH1-AS1 in pan-cancer and HCC was calculated using the R package "ggplot2". The subcellular localization of RNASEH1-AS1 was predicted by the lncATLAS online tool (https://lncatlas.crg.eu/) [18]. HCC patients were divided into two groups for each clinical characteristics according to Supplementary Table 2, the RNASEH1-AS1 expression were detected to evaluate the correlation between RNASEH1-AS1 and various clinicopathological features. HCC patients were divided into high expression group and low expression group according to the optimal cut-off value, and the overall survival (OS), disease specific survival (DSS) and progress free interval (PFI) between the two groups were inspected using R packages "Survival" and "Survminer". The Cox proportional hazards regression model was used to assess the risk factors affecting OS, and the nomogram prediction model and calibration plot were constructed using R package "rms" and "survival" to predict the 1-year, 3-year and 5-year OS rates of HCC patients based on risk factors that influence prognosis. Receiver operating characteristic (ROC) curves were created using the R package "pROC" to assess the diagnostic and prognostic performance.

Bioinformatics analysis of the correlation between RNASEH1-AS1 expression and immune cell infiltration

The correlation between RNASEH1-AS1 and the degree of immune cell infiltration in HCC was assessed based on TCGA data by single-sample GSEA (ssGSEA) algorithm using the R package "GSVA" [19]. HCC patients were divided into high and low expression groups according to the median expression of RNASEH1-AS1, and enrichment score between the two groups were determined using the R package "ggplot2".

Bioinformatics analysis of positively co-expressed genes of RNASEH1-AS1 in HCC

Genes positively co-expressed with RNASEH1-AS1 in HCC were obtained through batch analysis of the correlation between RNASEH1-AS1 and 19448 coding genes (|Spearman's r| >0.4 and adjusted *P* value <0.01) and were then adopted to perform GO and KEGG enrichment analysis by the R package "clusterProfiler". The top 10 hub genes were screened out by constructing protein-protein interaction (PPI) network using STRING online tools (www.stringdb.org) and Cytoscape software, and their expression and clinical significance in HCC were assessed using the above methods for analyzing RNASEH1-AS1.

Construction and evaluation of a prognostic model based on positively co-expressed genes of RNASEH1-AS1

Univariate Cox analysis of the OS of the top 10 positively co-expressed hub genes of RNASEH1-AS1 was conducted. The least absolute selection operator (LASSO) Cox penalized regression analysis was performed using the R package "glmnet" based on the genes associated with OS, and the genes with non-zero coefficients were selected to build a risk score prognostic signature. The risk score was constructed as follows:

$$\text{RiskScore} = \sum_{i=1}^{N} (exp \times coef)$$

Where *N* is the number of model genes; *exp* represents the expression value of genes; *coef* is the coefficient of each gene. Then, HCC patients were divided into high-risk and low-risk groups according to the median risk score, and Kaplan-Meier analysis was conducted to evaluate differences in OS between the two groups. ROC curve was generated to evaluate the diagnostic and prognostic performance of the risk model for HCC. The Cox regression model was used to evaluate whether risk score was an independent risk factor for OS in HCC, and the nomogram prediction model and calibration plot were constructed to predict the 1-year, 3-year and 5-year OS rates of HCC patients based on risk score.

Human HCC samples

A total of 20 samples of HCC tissues and matched neighboring noncancerous liver tissues were collected from patients who underwent surgical resection at Department of General Surgery, the Second Affiliated Hospital of Xi'an Jiaotong University between 2015 and 2017. All patients received written informed content and the study was permitted by the Ethics Committee of of Xi'an Jiaotong University Health Science Center (No. 2022-36).

Cell culture and transfection

Human normal liver cell line L-02 and six HCC cell lines (HepG2, Hep3B, Bel-7402, Bel-7404, MHCC97H, and SK-Hep-1) were purchased from the Cell Bank of Type Culture Collection of the Chinese Academy of Sciences (Shanghai, China). All cell lines were cultured in DMEM medium supplemented with 10% fetal bovine serum (FBS), penicillin 100 U/ml and streptomycin 100 μg/ml, and kept in a 37°C incubator with 5% CO_2. Small interfering RNA (siRNA) and plasmid were transfected by jetPRIME (Polyplus, France). All siRNAs were purchased from RiboBio (Guangzhou, China), and siRNA target sequences were as follows: siRNASEH1-AS1-1, GGCAGAGCAGUAGGACAAA; siRNASEH1-AS1-2, GCAGUAGGACAAAUAGCUA; siEIF4A3, AGACAUGACUAAAGUGGAA; siWDR12, CCUUGGAAGGAAAGUCAAUAA; siDKC1, CCGGCUGCACAAUGCUAUU; siNAT10, CGCAAAGUUGUGAAGCUAUUU. The DKC1 overexpression vector was purchased from Miaoling Bio (#P40631, Wuhan, China).

Quantitative real-time PCR (qRT-PCR)

Total RNA was extracted using Trizol reagent (Invitrogen, CA, USA) and reverse transcribed

using HiScript III 1st Strand cDNA Synthesis Kit (Vazyme, Nanjing, China). RNASEH1-AS1 were then detected by qRT-PCR using TB Green® Premix Ex Taq™ II reagent (TAKARA, Dalian, China) and GAPDH was used as the internal reference genes to perform relative quantitative analysis. Primers were shown as follows: RNASEH1-AS1, 5'-GCGGATCTACAGTAAGGGCTGT-3' and 5'-CGCCCTCCTTTGTGCTTATTC-3'; EIF4A3, 5'-GGCACAGGAAAAACAGCCACCT-3' and 5'-TGTAGTCACCGAGAGCAAGCAG-3'; WDR12, 5'-CTGCCTCTGAAATTGCCGACCT-3' and 5'-CCAAGGGCATTCGCAGAAACTG-3'; DKC1, 5'-AGTTGTGAGGCTGGCACCTACA-3' and 5'-ACAGCCACTGAGCATCAAGCAC-3'; NAT10, 5'-GGATTGCCTCAACATCACTCGG-3' and 5'-CGTTGGAGGAAAACTTCAGAGGC-3'; GAPDH, 5'-CCCTTCATTGACCTCAACTACATG-3' and 5'-TGGGATTTCCATTGATGACAAGC-3'.

Cell viability assay

Cells (5×10^3 cells/well) were paved in 96-well plates and incubated with CCK-8 reagent (Dojindo, Japan) for 1 h 30 min at 37°C. The optical density (OD) was collected at 450 nm by multifunctional microplate reader.

Colony formation assay

Cells were placed in 6-well plates at the density of 800 cells per well and cultured in complete medium for 7 days. When visible colonies appeared, the cells were fixed with 4% paraformaldehyde for 20 min. After staining with 0.1% crystal violet, the colonies were imaged and counted.

Transwell assay for cell migration and invasion detection

The capability of cell migration and invasion were assessed using Matrigel-uncoated and coated 24-well transwell chambers with 8.0 μm transparent PET membrane (353097 and 354480, Corning, USA), respectively. A total of 5×10^4 cells were resuspended in 200 μl of serum-free medium and seeded in the upper chamber. The culture medium was supplemented with 10% FBS as a chemoattractant and then added to the lower chamber. After 24 h (migration assay) or 48 h (invasion assay) of culture, the cells inside the chamber were wiped off and the cells outside the chamber were fixed with 4% paraformaldehyde. Subsequently, the migrated and invasive cells were stained with crystal violet and recorded under the microscope (100 ×) for counting.

Subcutaneous tumor-bearing experiment in nude mice

Female BALB/c nude mice (four-week-old) were purchased and raised in the Laboratory Animal Center of Xi'an Jiaotong University. Mice were randomly categorized into two groups (n=5 for each group). 150 μl of RNASEH1-AS1-silenced or negative control Bel-7404 cells (containing 4×10^6 cells) were subcutaneously injected in the right flank of each nude mouse. The length and width of the tumors were checked every 7 days using vernier caliper and the volumes were evaluated according to the formula: volume = (length × width^2)/2. At the end of the experiment, the mice were sacrificed, and the tumors were peeled off and weighed. All animal experiments were approved by the Animal Experimentation Ethics Committee of Xi'an Jiaotong University and were conducted in accordance with the institutional guidelines for care and use of laboratory animals.

RNA immunoprecipitation (RIP) assay

RIP assay was performed using the PureBinding®RNA Immunoprecipitation Kit (#P0101, Geneseed, Guangzhou, China) in accordance with the manufacturer's instructions. Briefly, 1×10^7 of cells were dissociated in Immunoprecipitation Lysis Buffer containing RNase and protease inhibitor; add 5 μg of anti-DKC1 antibody (Cloud-Clone, PAC446Hu01) or Rabbit Normal IgG (CST, 2729S) which have been bound to Protein A/G Magnetic Beads, and then incubated at 4°C for 2 hours; the RNA immunoprecipitated with the beads was isolated and further analyzed by qRT-PCR.

RNA pull-down assay

The sense and antisense DNA fragments of RNASEH1-AS1 containing the T7 promoter were synthesized by Genewiz (Suzhou, China). Biotin-labeled sense and antisense transcripts of RNASEH1-AS1 was transcribed *in vitro* by T7 High Yield RNA Synthesis Kit (Yeasen, Shanghai, China) using biotin-16-UTP (APExBIO, USA). 50 pmol biotin-labeled RNA was used to perform pull-down assay to enrich RNA-binding protein using the Pierce™ Magnetic RNA-

Protein Pull-Down Kit (#20164, Thermo scientific) as described by the manufacturer. The DKC1 was detected via western blot using anti-DKC1 antibody (1:1000; Cloud-Clone, PAC446Hu01).

RNA stability assay

24 h after transfection, cells were incubated with actinomycin D (2.5 μg/ml) for 2 h, 4 h, 6 h and 8 h. Cells without actinomycin D treatment were used as 0 h control. Total RNA was extracted and analyzed by qRT-PCR to evaluate RNASEH1-AS1 stability.

Statistical analysis

For bioinformatics analysis, statistical analyses were conducted using R (v.4.2.1). The expression differences of RNASEH1-AS1 in unpaired and paired tissues were analyzed by conducting the Mann-Whitney U test and Wilcoxon signed rank test, respectively. The association between RNASEH1-AS1 and clinical features was evaluated by the Mann-Whitney U test. Survival analysis was performed by log-rank test. The correlation between two genes was determined by the Spearman correlation test.

For wet-lab experiments, statistical analyses were conducted using SPSS 20.0. The data are expressed as the means ± standard deviation (SD). The differences between the two groups and multiple groups were determined by Student's t-test and one-way analysis of variance (ANOVA), respectively. $P<0.05$ was considered statistically significant.

Results

RNASEH1-AS1 was up-regulated in HCC based on TCGA data

To explore the expression status of RNASEH1-AS1 in HCC patients, the expression levels of RNASEH1-AS1 in 370 HCC tissues and 50 normal tissues, as well as 50 paired HCC tissues were first examined based on TCGA data, and the results showed that the expression level of RNASEH1-AS1 in tumor tissues were significantly higher in both unpaired and paired samples (both $P<0.001$) (**Figure 1A**, **1B**). Next, the expression of RNASEH1-AS1 in HCC tissues was further verified using GEO data, and RNASEH1-AS1 in tumor tissues was also found to be dramatically higher than those in normal tissues in four validation GEO datasets (both $P<0.05$) (**Figure 1C-F**). The prediction results of subcellular localization by lncATLAS showed that RNASEH1-AS1 was predominantly distributed in the cytoplasm for most cell types, including HCC cell line HepG2 (**Figure 1G**). In addition, the expression of RNASEH1-AS1 in pan-cancer was further investigated based on 30 types of TCGA tumors. As shown in **Figure 1H**, RNASEH1-AS1 was up-regulated in 22 cancer types including BRCA, CHOL, COAD, DLBC, ESCA, GBM, HNSC, KIRP, LGG, LIHC, LUAD, LUSC, OV, PAAD, PRAD, READ, SKCM, STAD, TGCT, THYM, UCEC and UCS, while was down-regulated in KICH, KIRC, LAML and THCA, indicating RNASEH1-AS1 was abnormally activated in the vast majority of tumor types.

Association between RNASEH1-AS1 expression and clinical characteristics of HCC patients

As shown in **Figure 2A**, **2B**, high RNASEH1-AS1 levels in HCC tissues were significantly positively associated with histological grade and AFP level (both $P<0.05$). As shown in **Figure 2C-E**, the overall survival (OS), disease specific survival (DSS) and progress free interval (PFI) of patients with high levels of RNASEH1-AS1 were significantly lower than those of patients with low expression (both $P<0.05$), suggesting that high RNASEH1-AS1 level was a poor prognostic factor in HCC. Univariate Cox regression analysis showed that RNASEH1-AS1 level (HR=1.492, $P=0.023$) and T stage (HR=2.583, $P<0.001$) were significantly correlated with the OS of HCC patients (**Figure 2F**). Multivariate Cox regression analysis further revealed that RNASEH1-AS1 levels (HR=1.479, $P=0.030$) was an independent risk factor affecting the OS of HCC patients (**Figure 2G**). In addition, a nomogram prediction model was constructed by integrating RNASEH1-AS1 level and key clinical characteristics (age, gender, histological grade, and T/N/M stage) to predict the 1-, 3-, and 5-year OS rates of HCC patients (**Figure 2H**), and the nomogram was demonstrated to have good accuracy and stability when assessed with a calibration test (**Figure 2I**).

Evaluation of the diagnostic and prognostic value of RNASEH1-AS1 in HCC

To evaluate the diagnostic value of RNASEH1-AS1 levels for HCC, the receiver operating char-

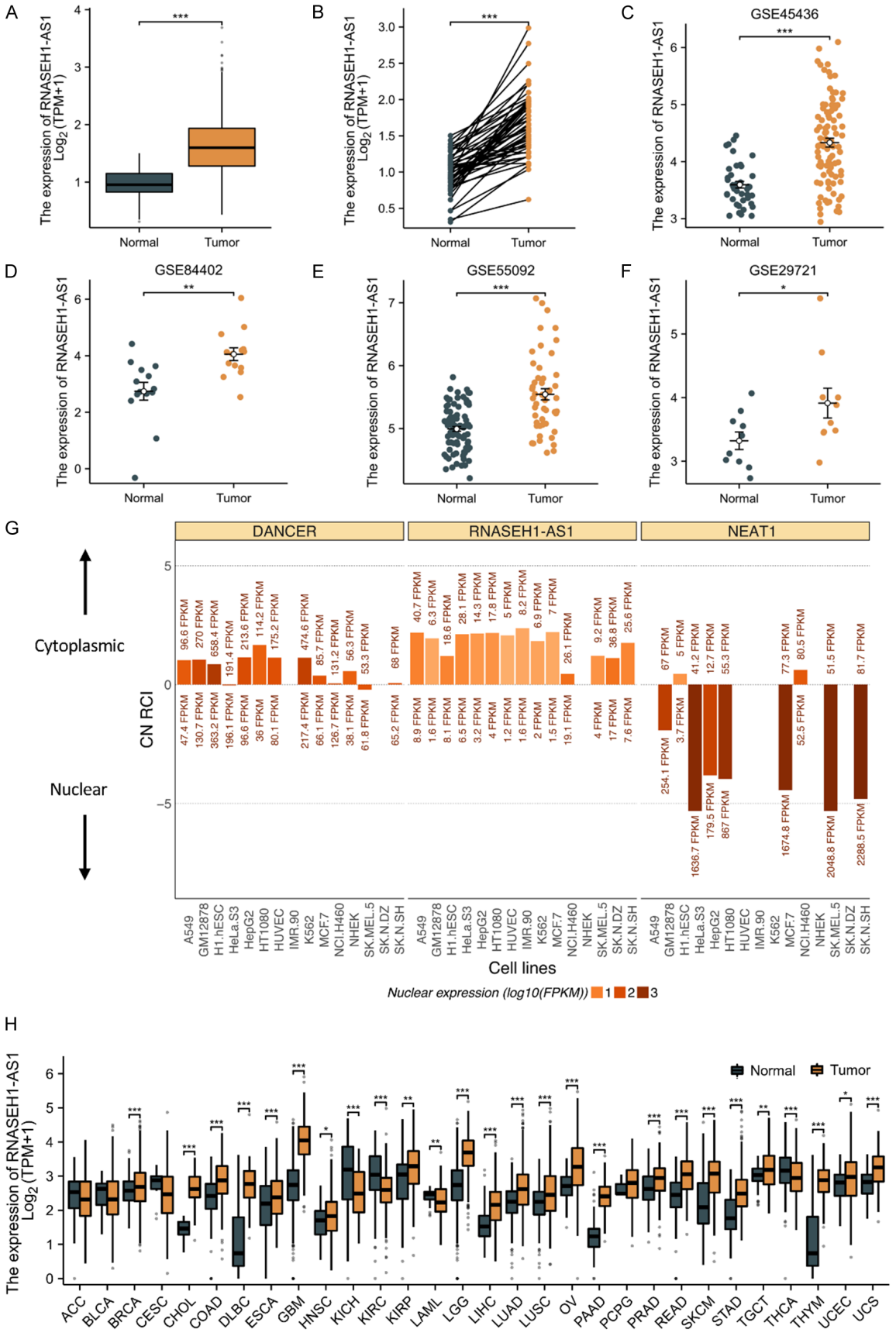
A
B
C
D
E
F
G
H
The expression of RNASEH1-AS1 Log2 (TPM+1)
Normal
Tumor
GSE45436
GSE84402
GSE55092
GSE29721
DANCER
RNASEH1-AS1
NEAT1
Cytoplasmic
Nuclear
CN RCI
Cell lines
Nuclear expression (log10(FPKM))
ACC
BLCA
BRCA
CESC
CHOL
COAD
DLBC
ESCA
GBM
HNSC
KICH
KIRC
KIRP
LAML
LGG
LIHC
LUAD
LUSC
OV
PAAD
PCPG
PRAD
READ
SKCM
STAD
TGCT
THCA
THYM
UCEC
UCS

Figure 1. RNASEH1-AS1 was up-regulated in HCC. RNASEH1-AS1 expression in unpaired (A) and paired (B) HCC tissues were analyzed using TCGA data and validated in four GEO datasets (C-F). (G) The subcellular localization of RNASEH1-AS1 in various cell types was predicted by lncATLAS. (H) Pan-cancer analysis of RNASEH1-AS1 expression across 30 cancer types based on TCGA data. *P<0.05, **P<0.01, ***P<0.001. ACC, adrenocortical carcinoma; BLCA, bladder urothelial carcinoma; BRCA, breast invasive carcinoma; CESC, cervical squamous cell carcinoma; CHOL, cholangiocarcinoma; COAD, colon adenocarcinoma; DLBC, diffuse large B-cell lymphoma; ESCA, esophageal carcinoma; GBM, glioblastoma multiforme; HNSC, head and neck squamous cell carcinoma; KICH, kidney chromophobe; KIRC, kidney renal clear cell carcinoma; KIRP, kidney renal papillary cell carcinoma; LAML, acute myeloid leukemia; LGG, brain lower grade glioma; LIHC, liver hepatocellular carcinoma; LUAD, lung adenocarcinoma; LUSC, lung squamous cell carcinoma; OV, ovarian serous cystadenocarcinoma; PAAD, pancreatic adenocarcinoma; PCPG, pheochromocytoma and paraganglioma; PRAD, prostate adenocarcinoma; READ, rectum adenocarcinoma; SKCM, skin cutaneous melanoma; STAD, stomach adenocarcinoma; TGCT, testicular germ cell tumors; THCA, thyroid carcinoma; THYM, thymoma; UCEC, uterine corpus endometrial carcinoma; UCS, uterine carcinosarcoma.

acteristic (ROC) curves was generated. As shown in **Figure 3A**, **3B**, RNASEH1-AS1 level has a good effect on the diagnosis of HCC (AUC=0.876) and histological stage G1&G2 (AUC=0.865). Furthermore, RNASEH1-AS1 level also showed good value for assessing 1-, 3-, and 5-year OS (AUC=0.619, 0.594, and 0.610, respectively), DSS (AUC=0.658, 0.606, and 0.587, respectively), as well as PFI (AUC= 0.619, 0.594, and 0.610, respectively) (**Figure 3C-E**).

Correlation of RNASEH1-AS1 level with immune cell infiltration in HCC

By analyzing the correlation between RNASEH1-AS1 level and infiltration levels of 19 types of immune cells in HCC tissues (**Figure 4A**), it was found that RNASEH1-AS1 level was negatively associated with the infiltration level of most detected immune cell types in HCC tumor microenvironment (|Spearman's r| >0.1, P<0.05) including pDC, B cells, neutrophils, iDC, Th1, Th17, macrophages, mast cells, Tgd, Treg, NK $CD56^{dim}$ cells, Tem, $CD8^{+}$ T cells, aDC, except for eosinophils, NK $CD56^{bright}$ cells, Tcm and Th2 cells (**Figure 4B**).

Prediction of potential mechanisms of RNASEH1-AS1 promoting HCC progression based on co-expression networks

To explore potential biological functions and pathways of RNASEH1-AS1 in HCC, a total of 1109 genes that were significantly positively co-expressed with RNASEH1-AS1 in HCC were screened out (|Spearman's r| >0.4, adjusted P value <0.01; Supplementary Table 3), then GO and KEGG enrichment analysis were performed and the top 10 most enriched terms for biological process (BP), cellular component (CC), molecular function (MF) as well as KEGG were obtained (**Figure 5A-D**; Supplementary Table 4). Combining the GO and KEGG enrichment results, we found the genes positively co-expressed with RNASEH1-AS1 are mainly related to RNA processing (splicing, methylation, localization), ribosome biogenesis, transcription, histone acetylation and so on, indicating RNASEH1-AS1 may participate in HCC progression by modulating above related biological processes and pathways.

To identify key co-expression genes of RNASEH1-AS1 in HCC, a protein-protein interaction (PPI) network was constructed based on positively co-expressed genes (PCEGs) of RNASEH1-AS1, the top 10 hub genes (EIF4A3, WDR43, WDR12, DKC1, NAT10, UTP18, DDX18, BYSL, DDX10, PDCD11) were recognized (**Figure 6A**) and their expression was highly positively correlated with RNASEH1-AS1 in HCC (**Figure 6B**, Supplementary Figure 1). Further analysis revealed that these hub genes were dramatically up-regulated in HCC and positively correlated with histological grade (both P<0.01) (Supplementary Figure 2), exhibiting a good diagnostic efficacy for HCC (both AUC>0.5) (Supplementary Figure 3). Except for DDX10, the expression levels of the remaining 9 hub genes were negatively associated with the OS of HCC patients (both P<0.05) (**Figure 6C**) and displayed certain predictive value for 1-, 3-, and 5-year overall survival (both AUC>0.5) (Supplementary Figure 4).

Construction and evaluation of a prognostic model based on hub genes of PCEGs

As shown in **Figure 6C**, 9 hub genes whose expression was significantly associated with worse OS were screened out, including EIF4A3, WDR43, WDR12, DKC1, NAT10, UTP18, DDX18, BYSL, and PDCD11. After LASSO regression

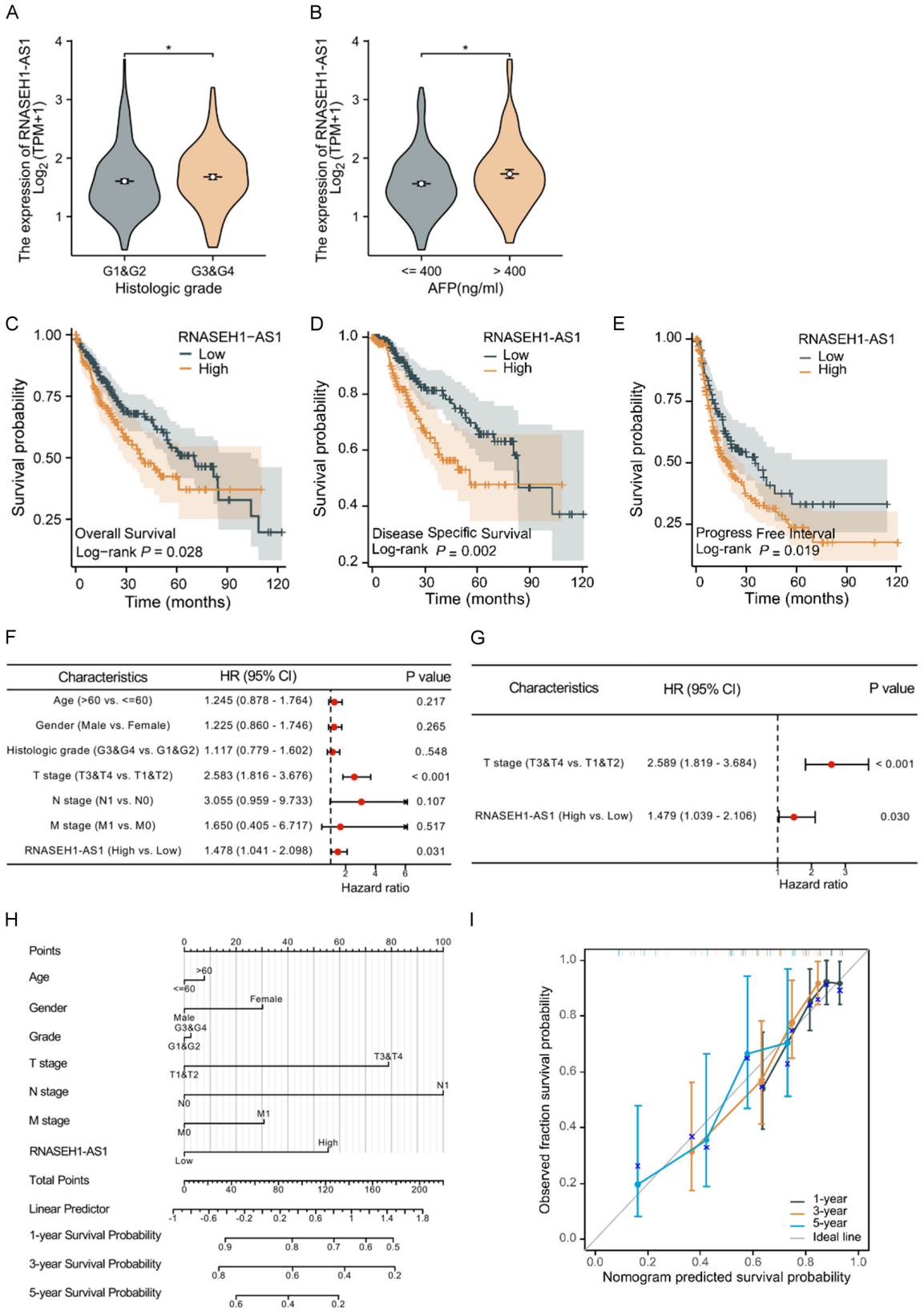

Figure 2. Association between RNASEH1-AS1 expression and clinical characteristics of HCC patients. Violin plot displaying the association between RNASEH1-AS1 expression and histological grade (A) and AFP level (B). Kaplan-Meier survival curves demonstrating relationship of RNASEH1-AS1 expression with overall survival (C), disease specific survival (D) and progress free interval (E). Forest plot showing results of univariate (F) and multivariate (G) Cox regression analysis of RNASEH1-AS1 level for overall survival. (H) The nomogram model predicting 1-, 3- and 5-year overall survival. (I) Calibration curves of the nomogram prediction model. *P<0.05.

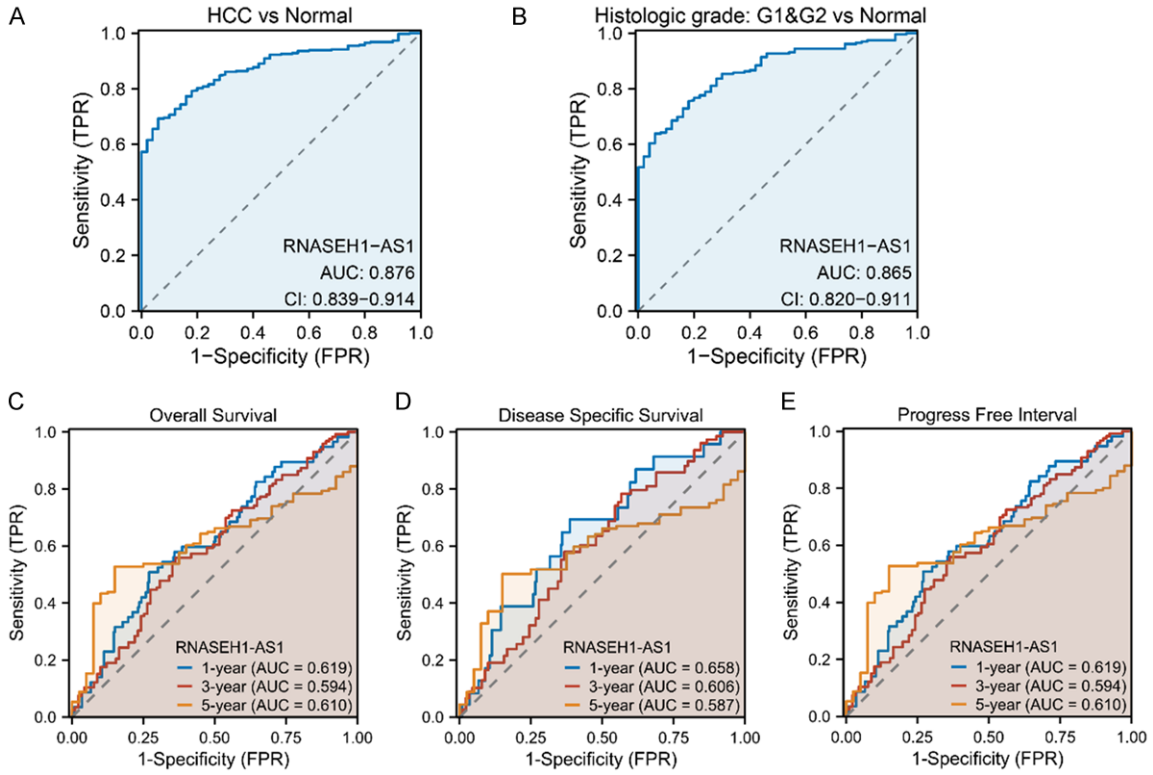

Figure 3. Diagnostic and prognostic ROC curves of RNASEH1-AS1 level in HCC. A. HCC vs. normal. B. Histologic grade G1&G2 vs. normal. C. 1-, 3-, and 5-year overall survival. D. 1-, 3-, and 5-year disease specific survival. E. 1-, 3-, and 5-year progress free interval.

analysis, a prognostic model was constructed using 4 hub genes (EIF4A3, WDR12, DKC1, NAT10) (**Figure 7A**, **7B**), and each patient's risk score were calculated following the formula: Risk score = expression level of EIF4A3 × 0.022 + expression level of WDR12 × 0.307 + expression level of DKC1 × 0.075 + expression level of NAT10 × 0.213. In order to evaluate the prognostic efficacy of this model, the patients were divided into a high-risk group and a low-risk group according to the threshold of median risk score. The distribution of risk scores, the relationship between survival time and risk score, as well as the clustering heatmap of the expression profile of four hub genes were shown in **Figure 7C**, and we found patients with high-risk scores had a higher mortality rate and shorter survival time compared with the low-risk group. Kaplan Meier curves also showed that patients in the high-risk group had a worse prognosis (P<0.05) (**Figure 7D**). Time-dependent ROC analysis disclosed that this model had a good prognostic accuracy for 1-, 3-, and 5-year overall survival (both AUC>0.6) (**Figure 7E**). Univariate and multivariate Cox regression analysis further revealed that the risk score was closely associated with OS of HCC patients and was an independent risk factor affecting the OS (HR=1.745, P=0.002) (**Figure 7F**, **7G**). Additionally, we established a nomogram prediction model combining risk score, age, gender, T, N, M, as well as histological grade, and the risk score was revealed to be an important factor among various clinical parameters (**Figure 7H**). As shown in **Figure 7I**, calibration curves showed that the nomogram model had a good predictive performance for 1-, 3-, and 5-year OS probability.

Experimental validation of the expression of RNASEH1-AS1 and its biological roles in HCC

To clarify the expression status of RNASEH1-AS1 in HCC, we detected the expression of RNASEH1-AS1 in twenty human HCC tissues and paired adjacent non-tumor tissues, as well as six HCC cell lines and human normal hepatocyte cell line L-02. As shown in **Figure 8A**, **8B**, the expression level of RNASEH1-AS1 in HCC tissues and HCC cell lines was signifi-

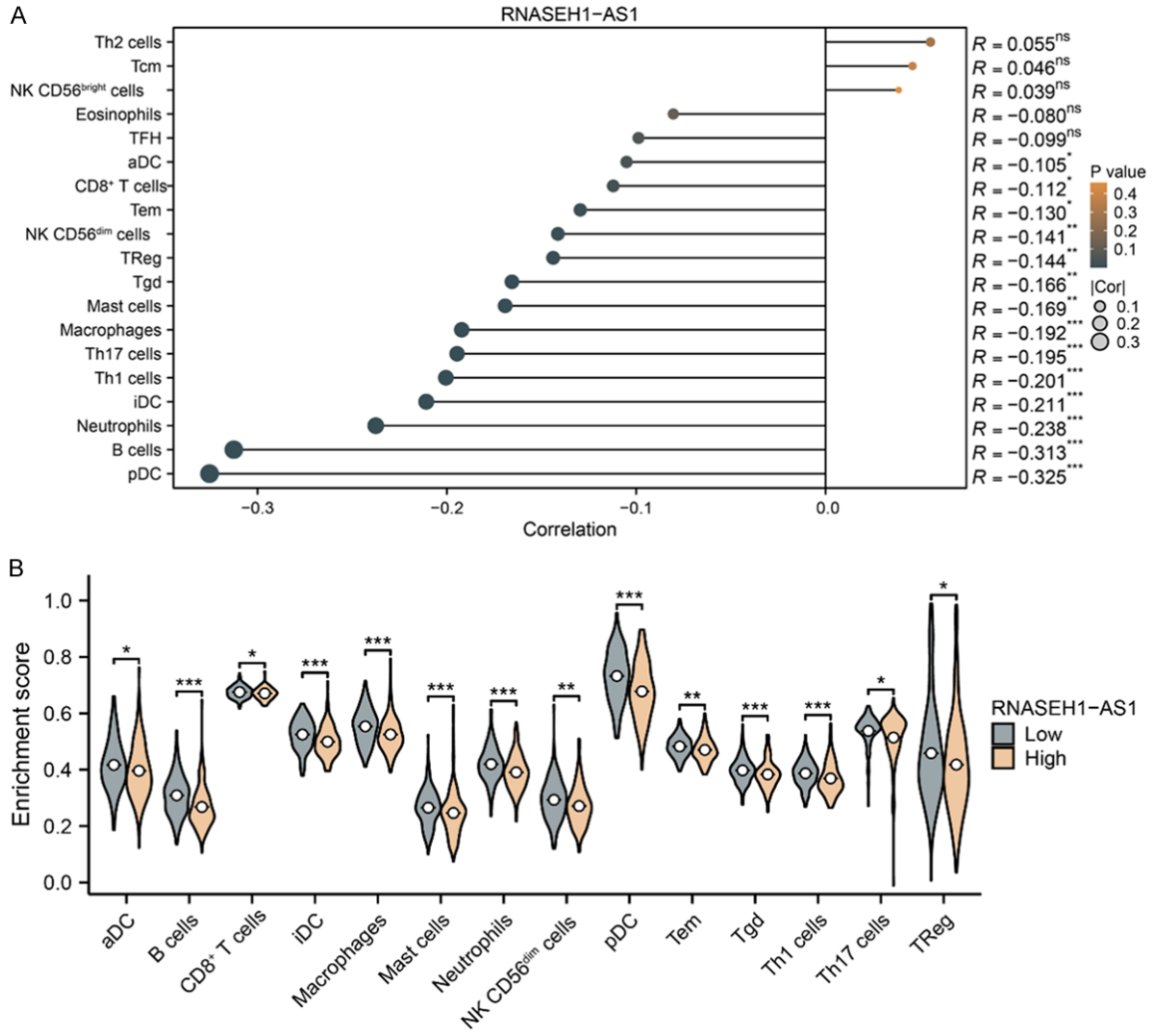

Figure 4. Relevance between RNASEH1-AS1 level and immune cell infiltration in HCC. A. Lollipop chart showing the correlation between RNASEH1-AS1 level and 19 different types of immune cells. B. Violin plot displaying the infiltration degree of 14 immune cell types in HCC patients with high and low expression of RNASEH1-AS1. *P<0.05, **P<0.01, ***P<0.001. aDC, activated dendritic cells; iDC, immature dendritic cells; pDC, plasmacytoid dendritic cells; NK, natural killer cells; Tcm, T central memory; Tem, T effector memory; TFH, T follicular helper cells; Tgd, gamma delta T cells; Th, T helper cells; Treg, regulatory T cells.

cantly higher than in paracancerous tissues and normal hepatocyte cell lines, which was consistent with the above bioinformatics findings.

To explore the biological functions of RNASEH1-AS1 in HCC, HepG2 and Bel-7404 cell lines which highly expressed RNASEH1-AS1 was selected to perform loss-of-function experiments (**Figure 8B**). The expression of RNASEH1-AS1 in HCC cells was knocked down by transfecting two siRNA and the effects of RNASEH1-AS1 knockdown on cell proliferation, migration and invasion were observed. As shown in **Figure 8C**, RNASEH1-AS1 could be successfully knocked down in both HepG2 and Bel-7404 cells by transfecting 50 nm siRNA. Based on the cell phenotype analysis *in vitro*, we found the capabilities of proliferation, colony formation, migration, and invasion of HCC cells were significantly suppressed upon RNASEH1-AS1 knockdown (**Figure 8D-G**). In addition, we conducted *in vivo* experiments using subcutaneous xenograft nude mouse model established by Bel-7404 cells and the results showed that the growth of xenograft tumors was significantly restrained after RNASEH1-AS1 knockdown (**Figure 8H-J**). Taken together, the above results indicated that RNASEH1-AS1 exerts a promoting role in HCC.

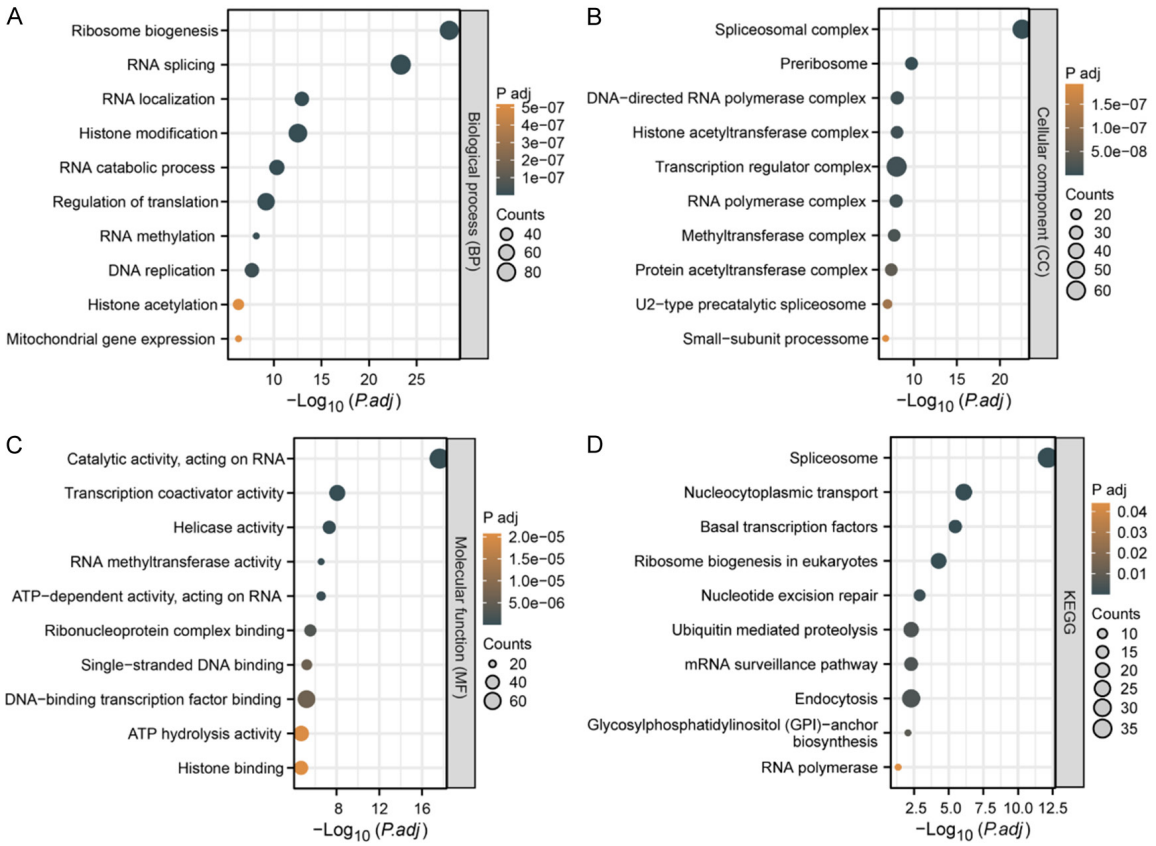

Figure 5. Functional enrichment analysis of genes significantly positively co-expressed with RNASEH1-AS1 in HCC. Bubble plot showing the top 10 enriched terms for biological process (A), cellular component (B), Molecular function (C) as well as KEGG (D).

RNASEH1-AS1 is regulated by DKC1 and mediates its cancer-promoting effects

To probe into the underlying mechanism of RNASEH1-AS1 promoting HCC progression, we detected the expression-regulation relationship between RNASEH1-AS1 and four hub genes (EIF4A3, WDR12, DKC1, NAT10) used to construct the prognostic model mentioned above, and the results showed that RNASEH1-AS1 knockdown had no effect on the expression of all four hub genes, while the expression of RNASEH1-AS1 expression was dramatically decreased only after silencing DKC1 (**Figure 9A**, **9B**), indicating RNASEH1-AS1 was a downstream gene of DKC1. Rescue experiments further demonstrated that RNASEH1-AS1 knockdown could retard the HCC-promoting effects of DKC1 (**Figure 9C-F**).

Dyskeratosis congenita 1 (DKC1), as an RNA-binding protein, has been demonstrated to directly bind to lncRNA and contribute to cancer progression by affecting RNA stability [20-22]. Here, to clarify whether DKC1 can interact with RNASEH1-AS1, RIP assay was first conducted and the results showed that the recovery of RNASEH1-AS1 was significantly higher in the complex with antibodies against DKC1 when compared with normal IgG (**Figure 9G**). In the RNA pull-down assay, we further found that DKC1 could be pulled down by the biotin-labeled RNASEH1-AS1 but not its antisense probe (**Figure 9H**). Besides, RNA stability assay revealed that the degradation rate of RNASEH1-AS1 was accelerated after DKC1 knockdown, indicating the stability of RNASEH1-AS1 can be modulated by DKC1 (**Figure 9I**). Collectively, the above results suggest that RNASEH1-AS1 can be controlled by DKC1 and mediates its HCC-promoting effects.

Discussion

HCC is a common malignant tumor with high morbidity and mortality and its clinical diagno-

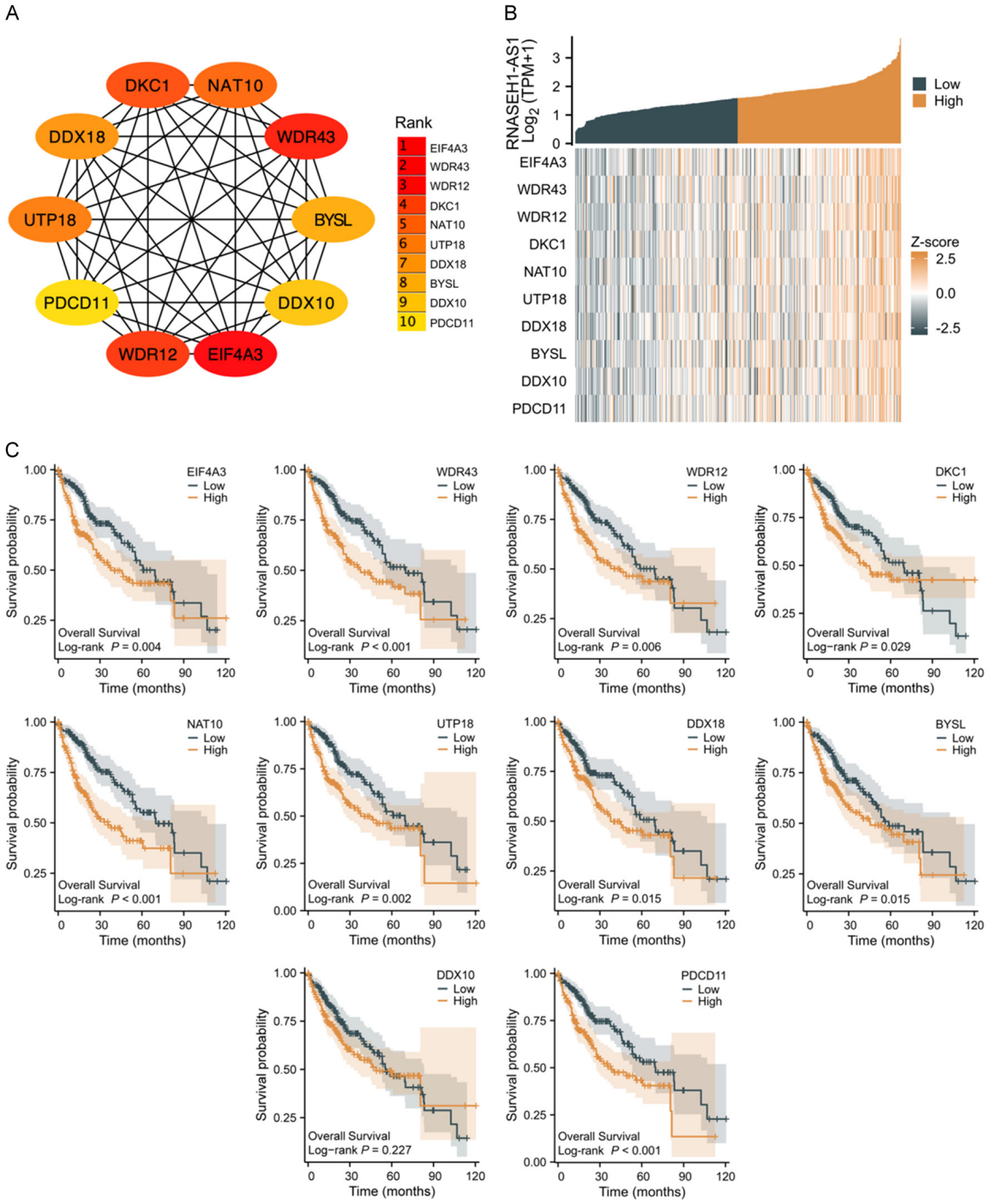

Figure 6. Construction of protein-protein interaction network based on positively co-expressed genes of RNASEH1-AS1 in HCC. A. The top 10 hub genes were identified based on the EPC methods. B. The correlation between the expression of hub genes and RNASEH1-AS1 in HCC was shown by heatmap. C. Correlation of hub genes expression with overall survival of HCC patients.

sis and treatment effect remain less than ideal due to the lack of effective early diagnosis methods as well as treatment strategies for intermediate-advanced HCC patients [23]. Benefiting from the rapid accumulation of tumor-related public data, bioinformatics mining of massive public omics data and clinical information have facilitated the development of novel tumor biomarkers and therapeutic targets.

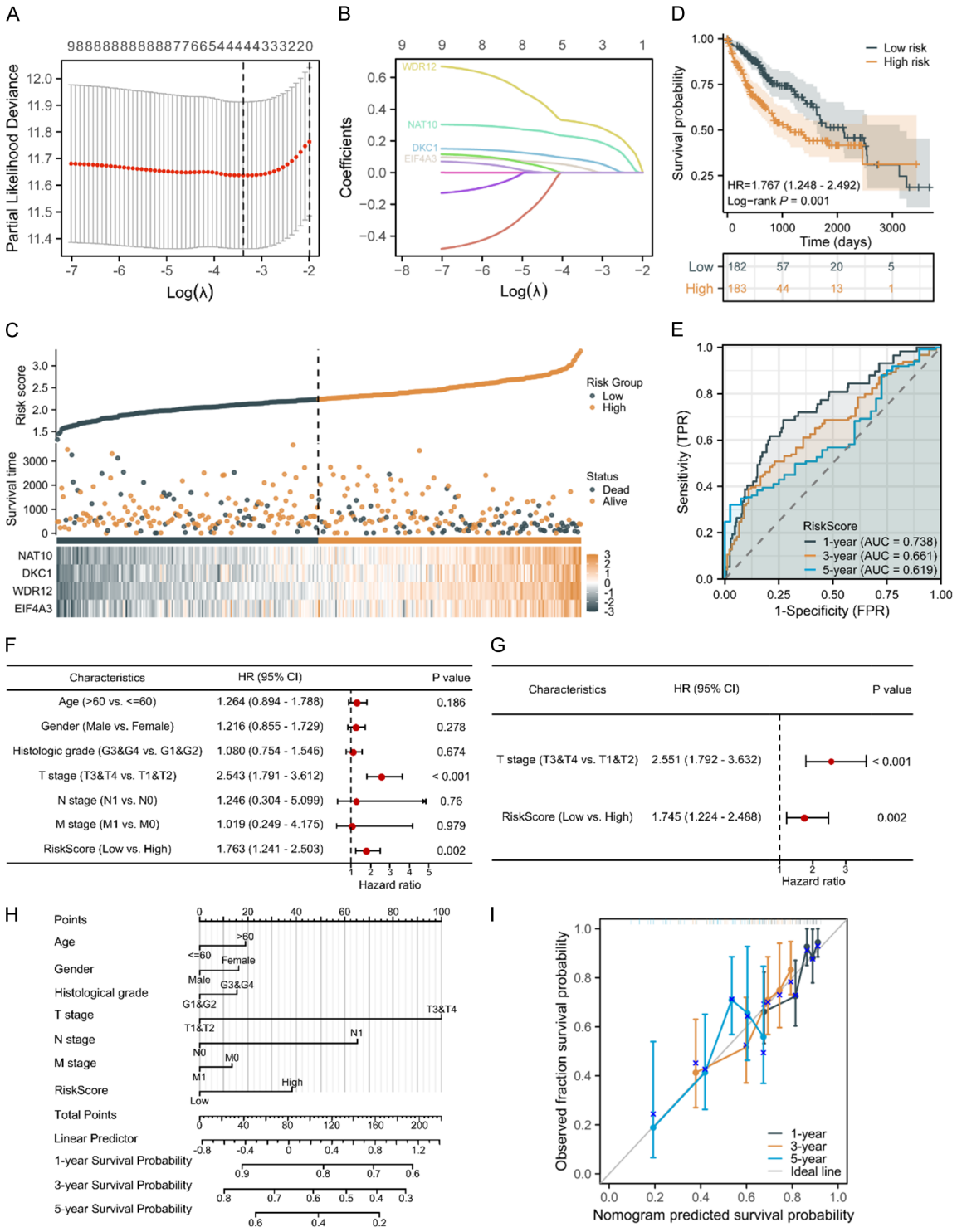

Figure 7. Construction of the HCC prognostic risk model based on 4 hub genes. (A) Cross-validation to select the optimal tuning parameter (λ). (B) LASSO coefficient profiles of the 9 hub genes. (C) The risk score, survival status, and expression heatmap of 4 hub genes in patients with HCC. (D) Kaplan Meier curves showing the overall survival of HCC patients in the high-risk and low-risk groups. (E) The predictive efficiency of the risk score for 1-, 3-, 5-year overall survival was verified by the ROC curve. Forest plot showing results of univariate (F) and multivariate (G) Cox regression analysis of the risk score for overall survival. (H) The Nomogram for predicting the 1-, 3-, and 5-year overall survival using the risk scores and clinical features in HCC. (I) Calibration plots for assessing the predictive performance of the nomogram.

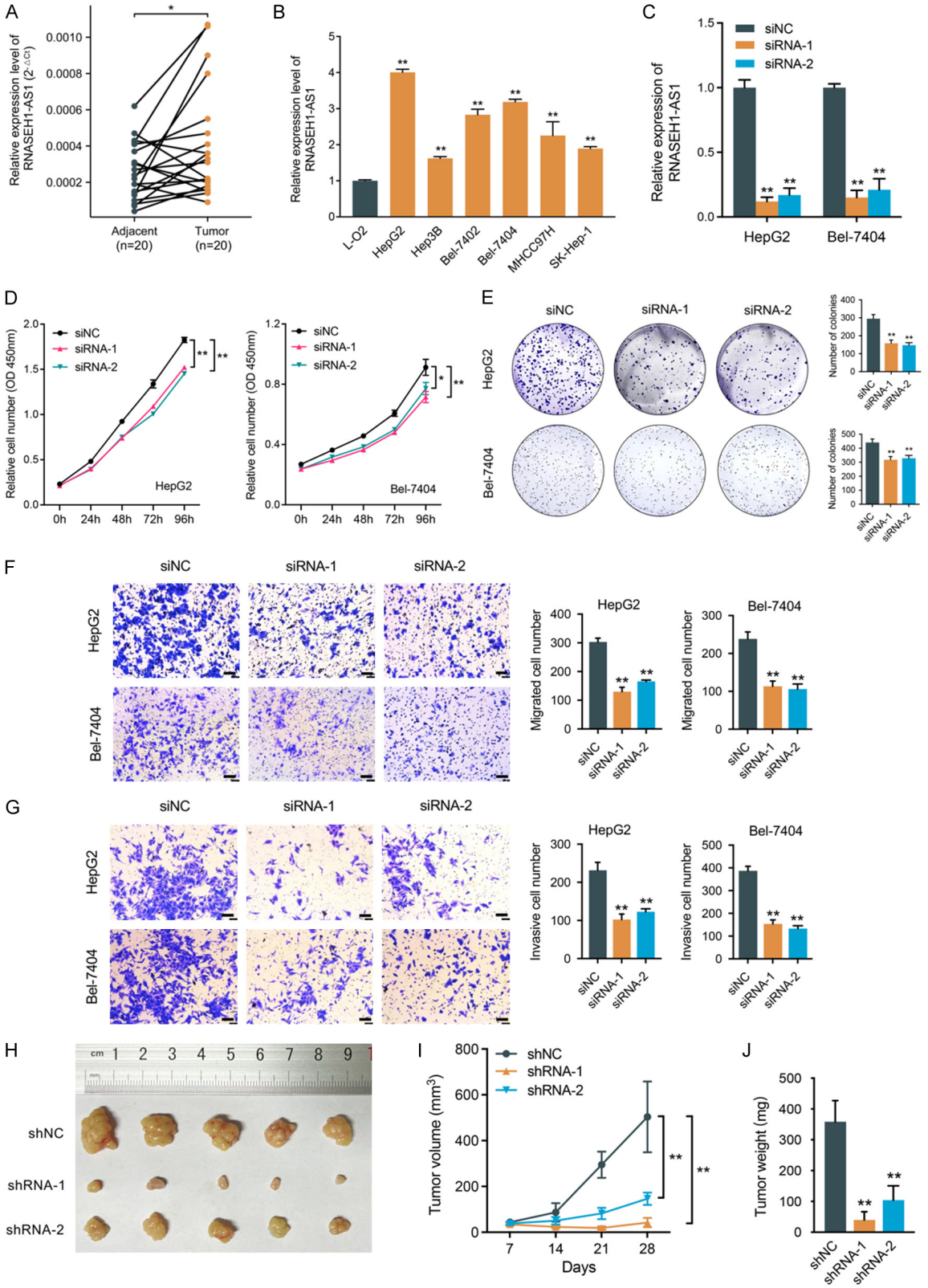

Figure 8. Experimental validation of the expression of RNASEH1-AS1 and its biological roles in HCC. Validation of the expression status of RNASEH1-AS1 in HCC tissues (A) and HCC cell lines (B) by qRT-PCR. (C) The knockdown efficiency of RNASEH-AS1 in HCC cells was evaluated by qRT-PCR. The proliferative ability of HCC cells was detected by CCK8 (D) and colony formation assay (E). The migration (F) and invasion (G) of HCC cells was assessed by transwell assay. (H) Photograph of dissected subcutaneous tumors at sacrificed time. (I) The volume of the subcutaneous tumors was measured every 7 days after implantation. (J) Tumor weight of dissected subcutaneous tumors at sacrificed time. Scale bar =100 μm. **P*<0.05, ***P*<0.01.

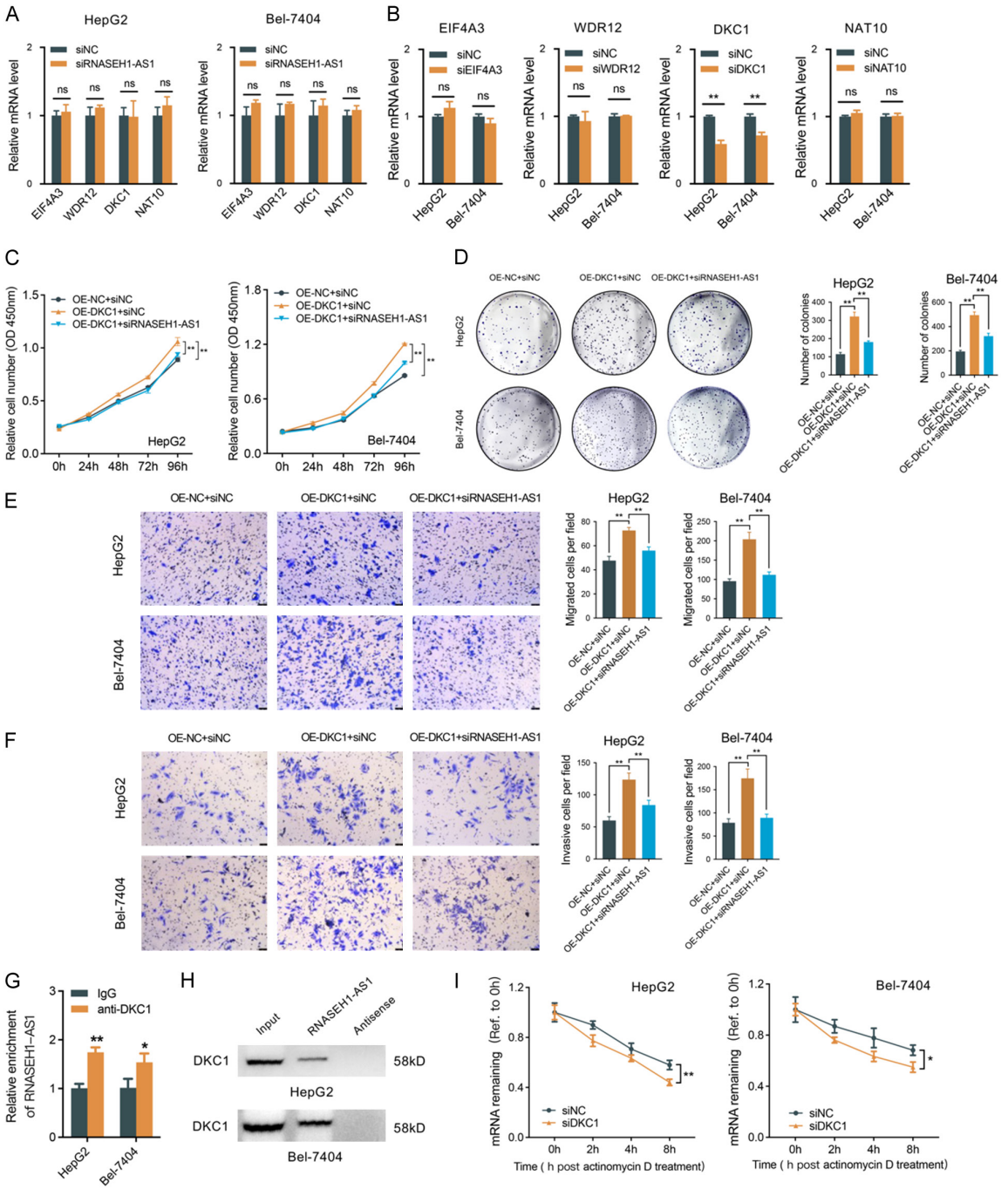

Figure 9. RNASEH1-AS1 is regulated by DKC1 and mediates its cancer-promoting effects. (A) The effects of RNASEH1-AS1 knockdown on the expression of four hub genes. (B) The effects of knockdown of four hub genes on the expression of RNASEH1-AS1. Knockdown of RNASEH1-AS1 attenuates the promoting effects of DKC1 overexpression on HCC cell proliferation (C, D), migration (E) and invasion (F). (G) RIP assay showed that RNASEH1-AS1 can be significantly enriched by the antibody of DKC1. (H) RNA pull-down assay showed that DKC1 can be pulled down by the biotin-labeled RNASEH1-AS1 but not its antisense probe. (I) RNA stability assay revealed that the degradation rate of RNASEH1-AS1 was accelerated after DKC1 knockdown. Scale bar =75 μm. *P<0.05, **P<0.01.

LncRNA, as a new type of regulatory molecule, has been proven to be widely involved in HCC progression and drug resistance in recent years, showing great potential as diagnostic marker and therapeutic target for HCC [24]. RNASEH1-AS1, an lncRNA transcribed from

human chromosome 2p25.3 region, has recently been revealed to be abnormally expressed in some tumors and involved in tumor progression. For example, RNASEH1-AS1, it has recently been demonstrated that overexpression of RNASEH1-AS1 in NSCLC is closely related to poor prognosis, and it can exacerbate cell growth and metastasis through regulating microRNA-516a-5p/FOXK1 axis and activating the Wnt/β-catenin signaling pathway [17]. However, it is still unclear whether RNASEH1-AS1 is linked to HCC. In the present study, the expression status of RNASEH1-AS1 and its potential clinical significance, biological function as well as mechanism of action in HCC were comprehensive analyzed by integrating bioinformatics strategies and experimental validation.

First, the high RNASEH1-AS1 level was found to be positively correlated with histological grade and AFP level of HCC patients, as well as worse OS, DSS, and PFI. Multivariate Cox regression analysis showed RNASEH1-AS1 was an independent risk factors affecting the OS of HCC patients. ROC curve analysis further revealed that RNASEH1-AS1 level had a good predictive effect on the HCC, histological grade G1&G2, OS, DSS and PFI, indicating that RNASEH1-AS1 has the potential to serve as a novel molecular marker for early diagnosis and prognosis of HCC.

Second, high expression of RNASEH1-AS1 was revealed to be negatively associated with the infiltration of most types of immune cells in HCC tissues, suggesting that RNASEH1-AS1 may be involved in the formation of immunosuppressive microenvironment of HCC, and the patients with high expression level of RNASEH1-AS1 may have poor sensitivity to immunotherapy. Here, it is worth noting that RNASEH1-AS1 has the most outstanding effect on the infiltration of pDC and B cells in HCC tissue. pDCs, as a dendritic cell subset, possess a distinct capacity to secrete high levels of type I INF-γ and have recently been found to be able to kill tumors directly by expressing tumor necrosis factor-related apoptosis-inducing ligand (TRAIL) and secreting granzyme B, as well as effectively enhancing the anti-tumor activity of NK and T cells [25]. B cells have also been demonstrated to have a positive correlation between their infiltration abundance and good clinical outcomes in tumor patients, and tumor-infiltrating B cells can inhibit tumor progression by affecting the activation of $CD8^+$ T cells, the secretion of antibodies and cytokines, and the facilitation of the antigen presentation [26].

Third, the potential roles and mechanism of RNASEH1-AS1 in HCC was explored based on its positively co-expressed genes. Notably, GO and KEGG enrichment analysis indicated RNASEH1-AS1-related genes were significantly enriched in several RNA processing-related terms, involving RNA splicing, RNA methylation, RNA localization. It is now known that divergent lncRNA can exert biological functions by positively regulating the expression of its neighbor coding genes, which is one of the main mechanisms of lncRNA action [27], whereas RNASEH1, as the divergent coding gene of RNASE1-AS1, has been shown to be associated with RNA processing [28]. Thus, RNASEH1-AS1 is highly likely to facilitate HCC progression by modulating RNASEH1. Ten hub genes were further identified through construction of PPI network, of which nine genes were significantly correlated with the OS of HCC patients. Furthermore, a prognostic risk model composed of four hub genes (EIF4A3, WDR12, DKC1, NAT10) was constructed by LASSO analysis, and the risk score calculated based on the model was an independent risk factor affecting OS, and exhibited good efficacy in predicting the prognosis of HCC patients. So far, EIF4A3, WDR12, DKC1, and NAT10 have all been revealed to be tightly related to HCC progression as oncogenes. EIF4A3, an ATP-dependent RNA helicase responsible for pre-mRNA splicing as component of the spliceosome, has been disclosed to be associated with worse survival and greater recurrence of HCC patients, and can facilitate HCC aggressiveness through modulating the splicing of FGFR4 [29]. WDR12, a crucial regulator of ribosome biogenesis, have been shown to be closely associated with high serum AFP level, vascular invasion, histologic grade and TNM stage of HCC patients, and knockdown of WDR12 can suppress the proliferation and migration of HCC cells [30]. DKC1, a key catalytic subunit responsible for rRNA pseudouracilation, was revealed to be positively correlated with serum AFP level, advanced clinical stage, and MYC expression of HCC patients [31]. NAT10, a nucleolar acetyltransferase involved in ribosome biogenesis, has recently

been found to be positively correlated with poor prognosis of HCC patients and accelerate the tumor metastasis and lenvatinib resistance through elevating the N4-acetocytidine (ac4C) modification level of HSP90AA1 mRNA [32].

Fourth, the expression status of RNASEH1-AS1 and its potential biological roles on HCC was determined by wet-lab experiments. We found that the expression of RNASEH1-AS1 in HCC tissues and cell lines was up-regulated, which was consistent with the TCGA data. Loss-of-function experiments further revealed that knockdown of RNASEH1-AS1 impaired the proliferation, migration and invasion ability of HCC cells, as well as the growth of subcutaneous tumors. Therefore, our results suggest that RNASEH1-AS1 plays a cancer-promoting role in HCC, similar to the findings in NSCLC [17].

Finally, the molecular mechanism of RNASEH1-AS1 in promoting HCC was further explored, and we demonstrated that the stability of RNASEH1-AS1 can be positively regulated by DKC1 via their direct interaction. DKC1 was previously found to catalyze pseudouridylation of rRNA as a subunit of H/ACA small nucleolar ribonucleoprotein (H/ACA snoRNP) complex [33]. In recent years, studies have uncovered that DKC1 can directly interact with lncRNA, for example PCAT1 in NSCLC cells and AC125611.3 in colon cancer cells [20, 22]. Pseudouridylation, as the most abundant RNA modification, is widely present in various RNA molecules, including lncRNA and can affect the RNA stability [33, 34]. Whether DKC1 maintains the stability of RNASEH1-AS1 discovered in this study is related to pseudouridylation remains to be further investigated.

Conclusions

The current study comprehensively revealed lncRNA RNASEH1-AS1 may serve as a potential prognostic, diagnostic biomarker as well as oncogenic gene for HCC, providing a theoretical basis for further basic and clinical translational research of RNASEH1-AS1.

Acknowledgements

This study was supported by the National Natural Science Foundation of China (No. 81502136); the Natural Science Foundation Research Program of Shaanxi Province of China (Nos. 2023-JC-YB-750 and 2022-JQ-938), and the Science Research Foundation of the Second Affiliated Hospital of Xi'an Jiaotong University (No. 2020YJ(ZYTS)546-09).

Disclosure of conflict of interest

None.

Address correspondence to: Zongfang Li, National and Local Joint Engineering Research Center of Biodiagnostics and Biotherapy, Xi'an Jiaotong University, No. 157 West 5th Road, Xi'an 710004, Shaanxi, China. Tel: +86-29-87679508; Fax: +86-29-87679508; E-mail: lzf2568@xjtu.edu.cn

References

[1] Sung H, Ferlay J, Siegel RL, Laversanne M, Soerjomataram I, Jemal A and Bray F. Global cancer statistics 2020: GLOBOCAN estimates of incidence and mortality worldwide for 36 cancers in 185 countries. CA Cancer J Clin 2021; 71: 209-249.

[2] Toh MR, Wong EYT, Wong SH, Ng AWT, Loo LH, Chow PK and Ngeow J. Global epidemiology and genetics of hepatocellular carcinoma. Gastroenterology 2023; 164: 766-782.

[3] Yang JC, Hu JJ, Li YX, Luo W, Liu JZ and Ye DW. Clinical applications of liquid biopsy in hepatocellular carcinoma. Front Oncol 2022; 12: 781820.

[4] Kamarajah SK, Bundred JR, Littler P, Reeves H, Manas DM and White SA. Treatment strategies for early stage hepatocellular carcinoma: a systematic review and network meta-analysis of randomised clinical trials. HPB (Oxford) 2021; 23: 495-505.

[5] Yan T, Yu L, Zhang N, Peng C, Su G, Jing Y, Zhang L, Wu T, Cheng J, Guo Q, Shi X and Lu Y. The advanced development of molecular targeted therapy for hepatocellular carcinoma. Cancer Biol Med 2022; 19: 802-817.

[6] Chen Y, Hu H, Yuan X, Fan X and Zhang C. Advances in immune checkpoint inhibitors for advanced hepatocellular carcinoma. Front Immunol 2022; 13: 896752.

[7] Mandlik DS, Mandlik SK and Choudhary HB. Immunotherapy for hepatocellular carcinoma: current status and future perspectives. World J Gastroenterol 2023; 29: 1054-1075.

[8] Mattick JS, Amaral PP, Carninci P, Carpenter S, Chang HY, Chen LL, Chen R, Dean C, Dinger ME, Fitzgerald KA, Gingeras TR, Guttman M, Hirose T, Huarte M, Johnson R, Kanduri C, Kapranov P, Lawrence JB, Lee JT, Mendell JT, Mercer TR, Moore KJ, Nakagawa S, Rinn JL,

Spector DL, Ulitsky I, Wan Y, Wilusz JE and Wu M. Long non-coding RNAs: definitions, functions, challenges and recommendations. Nat Rev Mol Cell Biol 2023; 24: 430-447.
[9] Statello L, Guo CJ, Chen LL and Huarte M. Gene regulation by long non-coding RNAs and its biological functions. Nat Rev Mol Cell Biol 2021; 22: 96-118.
[10] Mangiavacchi A, Morelli G and Orlando V. Behind the scenes: how RNA orchestrates the epigenetic regulation of gene expression. Front Cell Dev Biol 2023; 11: 1123975.
[11] Qian Y, Shi L and Luo Z. Long non-coding RNAs in cancer: implications for diagnosis, prognosis, and therapy. Front Med (Lausanne) 2020; 7: 612393.
[12] Khan A and Zhang X. Function of the long noncoding RNAs in hepatocellular carcinoma: classification, molecular mechanisms, and significant therapeutic potentials. Bioengineering (Basel) 2022; 9: 406.
[13] Verma S, Sahu BD and Mugale MN. Role of lncRNAs in hepatocellular carcinoma. Life Sci 2023; 325: 121751.
[14] Ge WJ, Huang H, Wang T, Zeng WH, Guo M, Ren CR, Fan TY, Liu F and Zeng X. Long noncoding RNAs in hepatocellular carcinoma. Pathol Res Pract 2023; 248: 154604.
[15] Wang Y, Yang F and Zhuang Y. Identification of a progression-associated long non-coding RNA signature for predicting the prognosis of lung squamous cell carcinoma. Exp Ther Med 2018; 15: 1185-1192.
[16] Zhao J, Song X, Xu T, Yang Q, Liu J, Jiang B and Wu J. Identification of potential prognostic competing triplets in high-grade serous ovarian cancer. Front Genet 2020; 11: 607722.
[17] Zhang C, Huang J, Lou K and Ouyang H. Long noncoding RNASEH1-AS1 exacerbates the progression of non-small cell lung cancer by acting as a ceRNA to regulate microRNA-516a-5p/FOXK1 and thereby activating the Wnt/beta-catenin signaling pathway. Cancer Med 2022; 11: 1589-1604.
[18] Mas-Ponte D, Carlevaro-Fita J, Palumbo E, Hermoso Pulido T, Guigo R and Johnson R. LncATLAS database for subcellular localization of long noncoding RNAs. RNA 2017; 23: 1080-1087.
[19] Hanzelmann S, Castelo R and Guinney J. GSVA: gene set variation analysis for microarray and RNA-seq data. BMC Bioinformatics 2013; 14: 7.
[20] Liu SY, Zhao ZY, Qiao Z, Li SM and Zhang WN. LncRNA PCAT1 interacts with DKC1 to regulate proliferation, invasion and apoptosis in NSCLC cells via the VEGF/AKT/Bcl2/Caspase9 pathway. Cell Transplant 2021; 30: 963689720986071.
[21] Chi Z, Sun Y, Yu Z, Zhou F, Wang H and Zhang M. Pseudogene fms-related tyrosine kinase 1 pseudogene 1 (FLT1P1) cooperates with RNA binding protein dyskeratosis congenita 1 (DKC1) to restrain trophoblast cell proliferation and angiogenesis by targeting fms-related tyrosine kinase 1 (FLT1) in preeclampsia. Bioengineered 2021; 12: 8885-8897.
[22] Tang H, Dou Y, Meng Y, Lu Q and Liang L. AC125611.3 promotes the progression of colon cancer by recruiting DKC1 to stabilize CTNNB1. Arab J Gastroenterol 2023; 24: 155-162.
[23] Llovet JM, Kelley RK, Villanueva A, Singal AG, Pikarsky E, Roayaie S, Lencioni R, Koike K, Zucman-Rossi J and Finn RS. Hepatocellular carcinoma. Nat Rev Dis Primers 2021; 7: 6.
[24] Sheng J, Lv E, Xia L and Huang W. Emerging roles and potential clinical applications of long non-coding RNAs in hepatocellular carcinoma. Biomed Pharmacother 2022; 153: 113327.
[25] Fu C, Zhou L, Mi QS and Jiang A. Plasmacytoid dendritic cells and cancer immunotherapy. Cells 2022; 11: 222.
[26] Zhang E, Ding C, Li S, Zhou X, Aikemu B, Fan X, Sun J, Zheng M and Yang X. Roles and mechanisms of tumour-infiltrating B cells in human cancer: a new force in immunotherapy. Biomark Res 2023; 11: 28.
[27] Luo S, Lu JY, Liu L, Yin Y, Chen C, Han X, Wu B, Xu R, Liu W, Yan P, Shao W, Lu Z, Li H, Na J, Tang F, Wang J, Zhang YE and Shen X. Divergent lncRNAs regulate gene expression and lineage differentiation in pluripotent cells. Cell Stem Cell 2016; 18: 637-652.
[28] Wu H, Sun H, Liang X, Lima WF and Crooke ST. Human RNase H1 is associated with protein P32 and is involved in mitochondrial pre-rRNA processing. PLoS One 2013; 8: e71006.
[29] Lopez-Canovas JL, Herman-Sanchez N, Moreno-Montilla MT, Del Rio-Moreno M, Alors-Perez E, Sanchez-Frias ME, Amado V, Ciria R, Briceno J, de la Mata M, Castano JP, Rodriguez-Peralvarez M, Luque RM and Gahete MD. Spliceosomal profiling identifies EIF4A3 as a novel oncogene in hepatocellular carcinoma acting through the modulation of FGFR4 splicing. Clin Transl Med 2022; 12: e1102.
[30] Yin Y, Zhou L, Zhan R, Zhang Q and Li M. Identification of WDR12 as a novel oncogene involved in hepatocellular carcinoma propagation. Cancer Manag Res 2018; 10: 3985-3993.
[31] Liu B, Zhang J, Huang C and Liu H. Dyskerin overexpression in human hepatocellular carcinoma is associated with advanced clinical stage and poor patient prognosis. PLoS One 2012; 7: e43147.
[32] Pan Z, Bao Y, Hu M, Zhu Y, Tan C, Fan L, Yu H, Wang A, Cui J and Sun G. Role of NAT10-mediated ac4C-modified HSP90AA1 RNA acetyla-

tion in ER stress-mediated metastasis and lenvatinib resistance in hepatocellular carcinoma. Cell Death Discov 2023; 9: 56.

[33] Schwartz S, Bernstein DA, Mumbach MR, Jovanovic M, Herbst RH, Leon-Ricardo BX, Engreitz JM, Guttman M, Satija R, Lander ES, Fink G and Regev A. Transcriptome-wide mapping reveals widespread dynamic-regulated pseudouridylation of ncRNA and mRNA. Cell 2014; 159: 148-162.

[34] Li X, Zhu P, Ma S, Song J, Bai J, Sun F and Yi C. Chemical pulldown reveals dynamic pseudouridylation of the mammalian transcriptome. Nat Chem Biol 2015; 11: 592-597.

Supplementary Table 1. The number of TCGA RNA-seq samples of 30 cancer types used for pan-cancer analysis

Cancer name	Tissue type	Number
ACC	Normal	128
ACC	Tumor	77
BLCA	Normal	28
BLCA	Tumor	407
BRCA	Normal	292
BRCA	Tumor	1099
CESC	Normal	13
CESC	Tumor	306
CHOL	Normal	9
CHOL	Tumor	36
COAD	Normal	349
COAD	Tumor	290
DLBC	Normal	444
DLBC	Tumor	47
ESCA	Normal	666
ESCA	Tumor	182
GBM	Tumor	1157
GBM	Normal	166
HNSC	Normal	44
HNSC	Tumor	520
KICH	Normal	53
KICH	Tumor	66
KIRC	Normal	100
KIRC	Tumor	531
KIRP	Normal	60
KIRP	Tumor	289
LAML	Normal	70
LAML	Tumor	173
LGG	Normal	1152
LGG	Tumor	523
LIHC	Normal	160
LIHC	Tumor	371
LUAD	Normal	347
LUAD	Tumor	515
LUSC	Normal	338
LUSC	Tumor	498
OV	Normal	88
OV	Tumor	427
PAAD	Normal	171
PAAD	Tumor	179
PCPG	Normal	3
PCPG	Tumor	182
PRAD	Normal	152
PRAD	Tumor	496
READ	Normal	318
READ	Tumor	93

SKCM	Normal	813
SKCM	Tumor	469
STAD	Normal	210
STAD	Tumor	414
TGCT	Normal	165
TGCT	Tumor	154
THCA	Normal	338
THCA	Tumor	512
THYM	Normal	446
THYM	Tumor	119
UCEC	Normal	101
UCEC	Tumor	181
UCS	Normal	78
UCS	Tumor	57

Supplementary Table 2. The clinical characteristics of 370 HCC patients obtained from the TCGA

Characteristic	Total (370)	%
Age (years)		
<=60	177	47.8
>60	193	52.2
Gender		
Female	121	32.7
Male	249	67.3
T stage		
T1&T2	274	74.7
T3&T4	93	25.3
N stage		
N0	251	98.4
N1	4	1.6
M stage		
M0	266	98.5
M1	4	1.5
Histologic grade		
G1-G2	232	63.6
G3-G4	133	36.4
AFP (ng/ml)		
<=400	214	77.0
>400	64	23.0

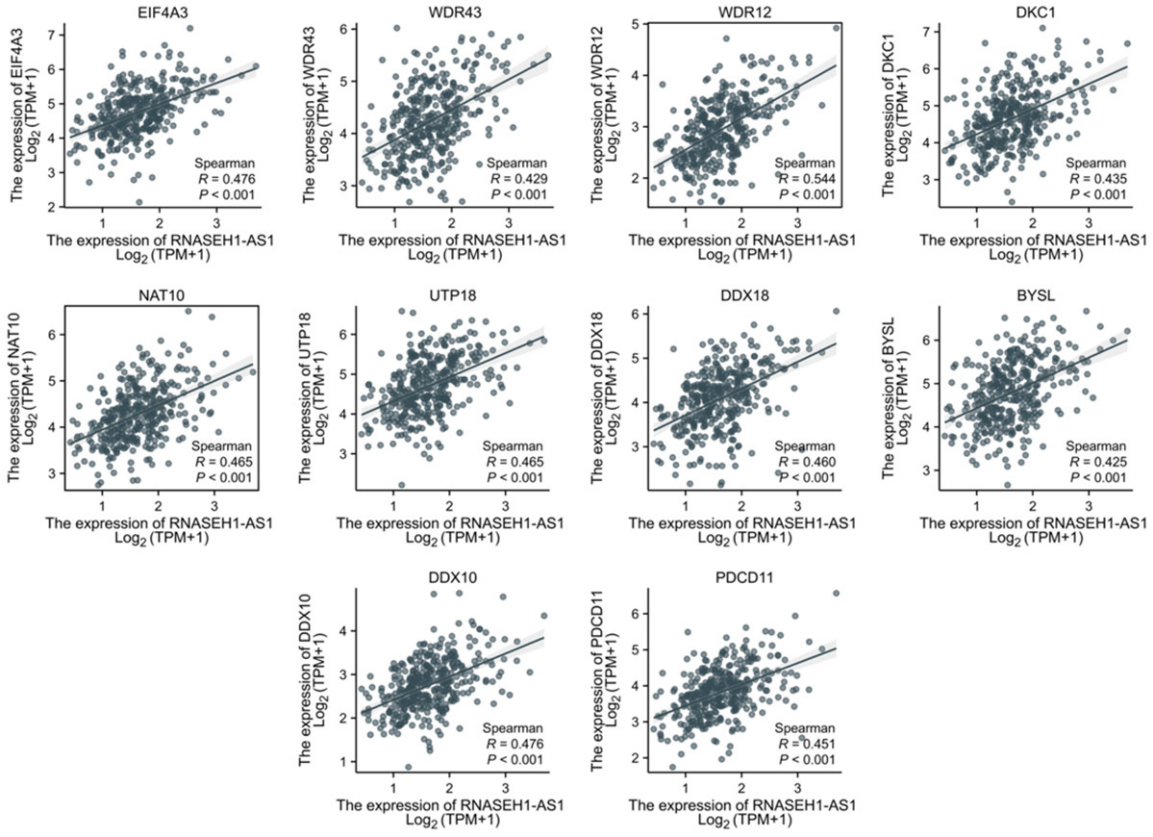

Supplementary Figure 1. The expression correlation between the top 10 hub genes and RNASEH1-AS1 in HCC was shown by scatter plots.

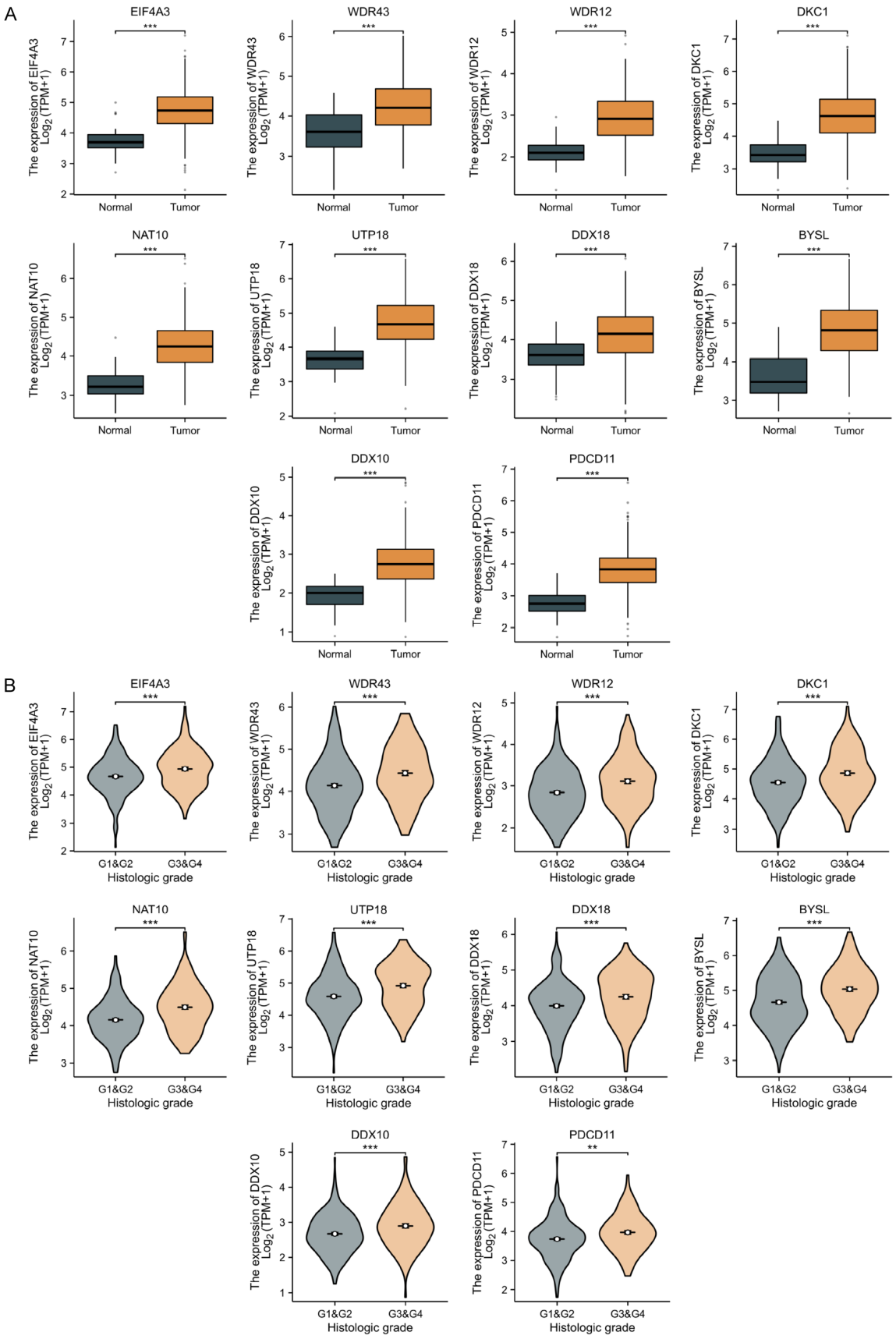

Supplementary Figure 2. The expression status of hub genes in HCC (A) and their correlation with histological grade (B). ***P*<0.01, ****P*<0.001.

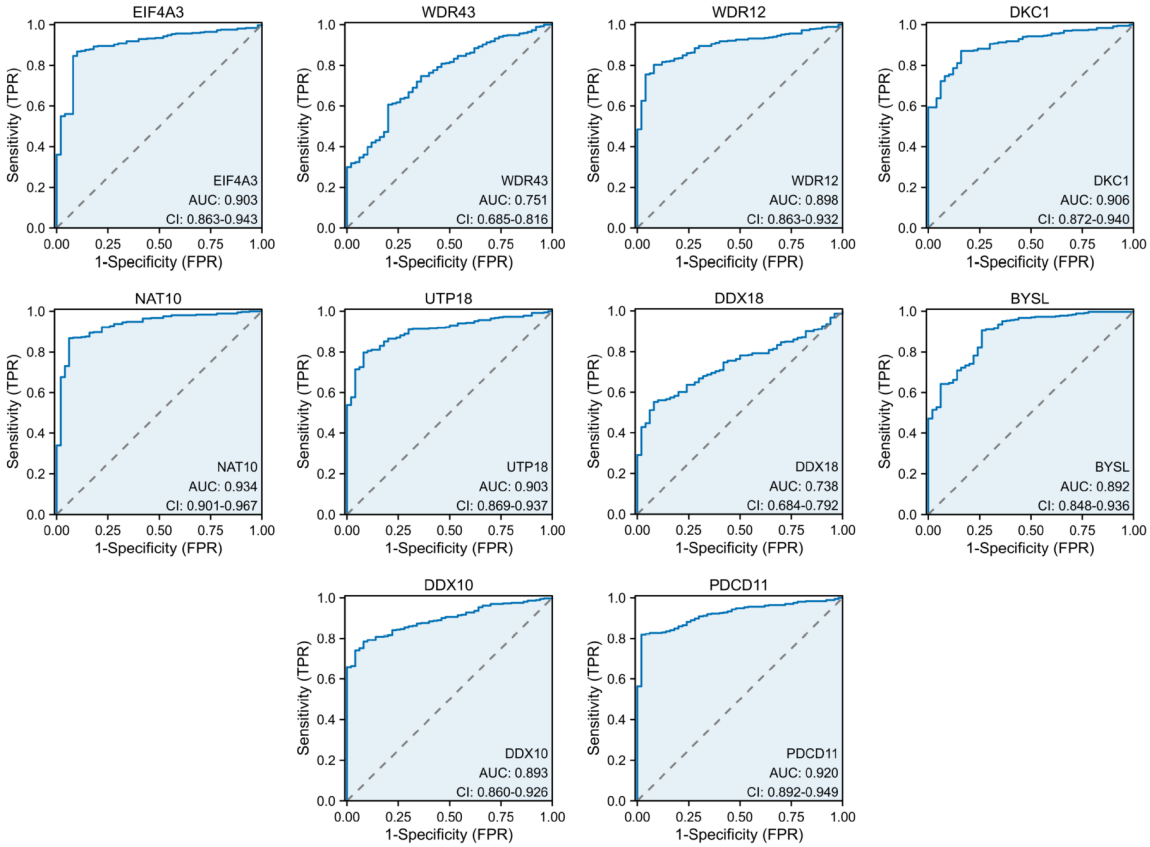

Supplementary Figure 3. ROC curves demonstrating the diagnostic value of the hub genes for HCC. AUC, area under the curve; CI, confidence interval; FPR, false-positive rate; TPR, true-positive rate.

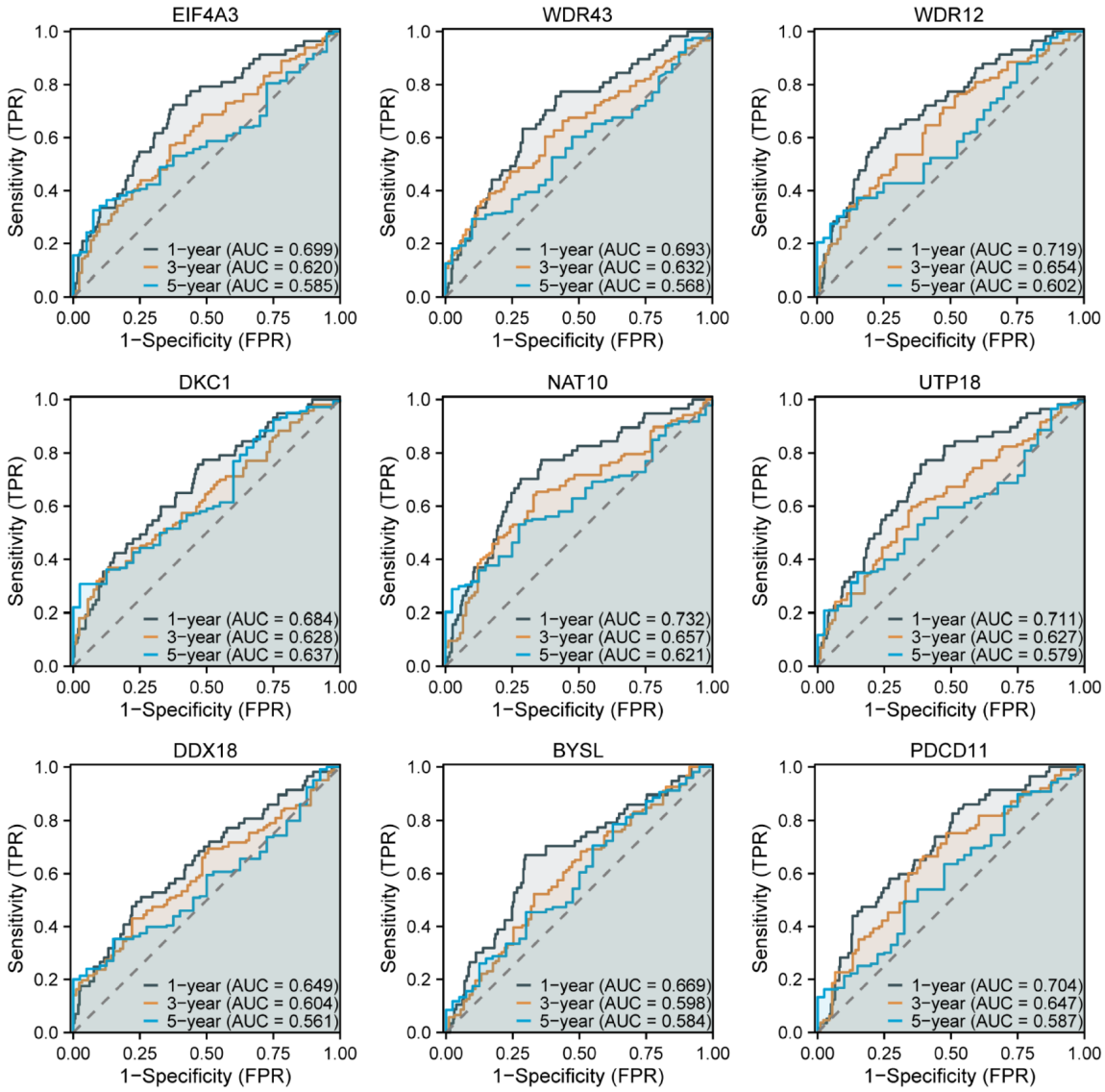

Supplementary Figure 4. ROC curves illustrating the predictive efficiency of the hub genes for 1-, 3-, 5-year overall survival of HCC patients. AUC, area under the curve; FPR, false-positive rate; TPR, true-positive rate.